Journal of the European Ceramic Society **10** (1992) 369–379

Si_3N_4–SiC Particulate Composites: Devitrification of the Intergranular Phase and its Effect on Creep

K. Ramoul-Badache & M. Lancin*

Physique des matériaux, CNRS, 1 Place A. Briand, 92195 Meudon Cedex, France

(Received 12 November 1991; revised version received 10 February 1992; accepted 13 February 1992)

Abstract

Pressureless sintered β'-Si_3N_4 materials containing either 0, 17 or 34 wt% of SiC and 10·5 wt% Al_2O_3 + 4·5 wt% Y_2O_3 additives were heat-treated to stabilize the microstructure by devitrification of their glassy intergranular phase. Heat-treatments at 1523 K result in the formation of YAG ($3Y_2O_3.5Al_2O_3$) and Y2S ($Y_2O_3.2SiO_2$). Using TEM and EDS characterizations, the nucleation of YAG or Y2S crystals was related to the presence or to the absence of SiC inclusions in the glassy interphase. At 1523 K, a complete devitrification cannot be achieved whatever the annealing time. SiC appears to increase devitrification and YAG formation. At 1573 K or 1623 K less complete devitrification occurs and only the YAG phase is detected. The creep resistance during compression tests at 1523 K is clearly increased by annealing but the residual glassy interphase still influences deformation.

Drucklos gesintertes β'-Si_3N_4-Material mit einem SiC-Gehalt von entweder 0, 17 oder 34 Gew.% und mit 10·5 Gew.% Al_2O_3–und 4·5 Gew.% Y_2O_3–Zusatz wurde wärmebehandelt, um das Gefüge durch die Kristallisation der glasartigen intergranularen Phase zu stabilisieren. Glühungen bei 1523 K führen zur Bildung von YAG ($3Y_2O_3.5Al_2O_3$) und von Y2S ($Y_2O_3.2SiO_2$). Das Gefüge wurde mittels TEM und EDS charakterisiert. Die Keimbildung von YAG- oder Y2S-Kristallen wird auf die Existenz oder das Fehlen von SiC-Einschlüssen in der glasartigen Phase zurückgeführt. Bei 1523 K kann auch nach sehr langen Anlaßzeiten keine vollständige Kristallisation beobachtet werden. SiC scheint die Kristallisation und die Bildung von YAG zu beschleunigen. Bei 1573 K und 1623 K ist die Kristallisation in noch geringerem Ausmaße abgelaufen und lediglich die YAG-Phase kann beobachtet werden. Wie Druckversuche bei 1523 K zeigen, kann die Kriechbeständigkeit durch Anlassen deutlich erhöht werden, auch wenn noch nicht auskristallisierte Glasphase in den Kornzwischenräumen das Verformungsverhalten beeinflußt.

Pour stabiliser la microstructure par dévitrification de la phase intergranulaire vitreuse, on a recuit des échantillons de β'-Si_3N_4, contenant soit 0, 17 ou 34% en poids de SiC. Ces matériaux avaient été frittés naturellement en présence d'ajouts (10·5% en poids de Al_2O_3 + 4·5% en poids de Y_2O_3). Les traitements thermiques à 1523 K provoquent la formation de YAG ($3Y_2O_3.5Al_2O_3$) et de Y2S ($Y_2O_3.2SiO_2$). Grace à des caractérisations par MET et EDS, on a relié la nucléation du YAG ou du Y2S à la présence ou à l'absence d'inclusion de SiC dans la phase intergranulaire vitreuse. A 1523 K, une dévitrification complète ne peut être obtenue quel que soit le temps de recuit. SiC accroit le taux de dévitrification et de formation de YAG. A 1573 K ou 1623 K, la dévitrification est moins complète qu'à 1523 K et seul le YAG est détécté. La résistance au fluage en compression à 1523 K est clairement augmentée par les recuits mais la phase vitreuse résiduelle joue toujours sur les mécanismes de déformation.

1 Introduction

Silicon nitrides have potential importance for structural applications because they combine refractoriness, chemical stability, resistance to corrosion

*To whom correspondence should be addressed at IMN, 2 rue de Houssinière, 44072 Nantes Cedex, France.

Journal of the European Ceramic Society 0955-2219/92/$5.00 © 1992 Elsevier Science Publishers Ltd, England. Printed in Great Britain

and low thermal expansion coefficients. However, both their creep resistance, which decreases as the temperature increases, and their brittleness limit their application. In an effort to enhance the mechanical properties of the materials, Si_3N_4-composites are being developed. Among these, composites that are obtained by including silicon carbide particles into a silicon nitride matrix seem to offer interesting outlets.[1,2]

In order to obtain maximum densification and for economy's sake, Si_3N_4 and its composites are sintered with some additives. Oxides such as MgO, Y_2O_3 or Al_2O_3 are most usually employed. Their reaction with ever-present silica on the surface of the Si_3N_4 grains results in the formation of a liquid interphase at the temperature of sintering and thus allows liquid-phase sintering.[3,4] Upon cooling, this liquid phase generally forms a silica glassy phase which is stabilized by impurities such as calcium.[5,6] Such an intergranular amorphous phase was formed in the Si_3N_4–SiC composites studied in this work (Fig. 1).[7] The influence of this glassy intergranular phase is catastrophic in regard to most of the applications of Si_3N_4 and its composites. Indeed, the softening of the glassy phase which occurs when the temperature increases results in grain sliding under stress[8,9] and in a rapid deterioration of the pieces.[10,11]

In order to reduce or even to avoid such a degradation two solutions may be proposed:

—An increase of the viscosity of the vitreous phase by changing its structure and its composition;

—a devitrification of the vitreous phase.

This paper reports results obtained while studying the efficiency of the second method. Two points will be then discussed:

(i) The devitrification of the glassy phase: firstly, the influence of the annealing conditions (t, T) on the devitrification of the composite containing 17 wt% of SiC are described. Then the influence of the SiC content on the devitrification is reported.

(ii) The influence of the devitrification on the creep behaviour of the Si_3N_4–SiC composites.

2 Materials

The process was detailed by Tanaka *et al.*[12] who provided the present authors with the composites.

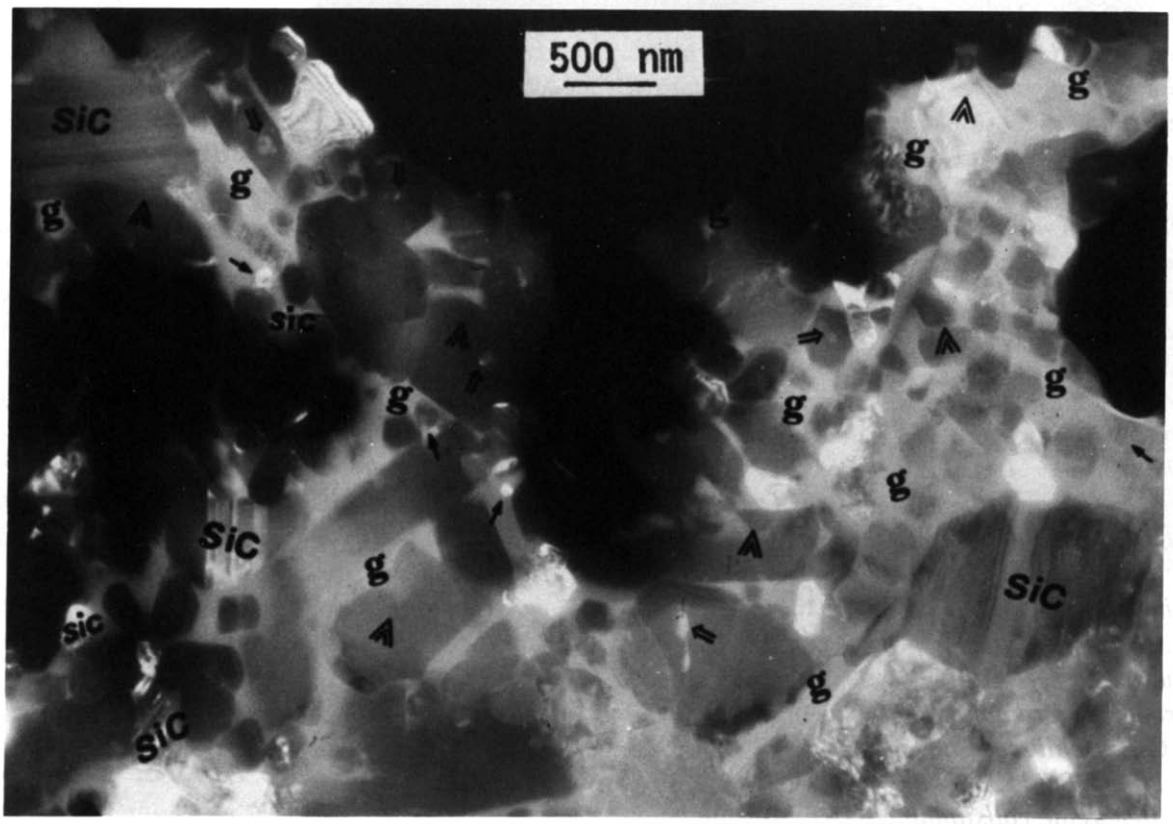

Fig. 1. Typical microstructure of the as-sintered composites. It is illustrated in a dark-field image of the SNC-17 composite (17 wt% SiC). Some grains are labelled on the figure: ≪, β'-Si_3N_4 grains with their faceted shape and their large range of size; SiC, large SiC grains with their stacking faults; → and ⇒, SiC inclusions in the glassy phase and in the β'-Si_3N_4 grains, respectively; g, glassy pockets or interphases.

Table 1. Characteristics of the composite.[12]

Samples	*SiC content (wt%)*	*Relative density (%)*
SN-0	0	96·0
SNC-17	17·0	92·0
SNC-34	34·0	91·7

Two fine-grained powders composed of either pure α-Si_3N_4 or pure β-SiC were used as starting materials. The mean grain size of the Si_3N_4 and of the SiC powders were equal to 0·5 and 1·0 μm respectively. The two powders were mixed with 10·5 wt% Al_2O_3 and 4·5 wt% Y_2O_3. This mixture was cold isostatically pressed under 630 MPa. The powder compacts were subsequently pressureless sintered in nitrogen atmosphere ($P_{N_2} = 0{\cdot}1$ MPa) at 2123 K for 1 h.

The Si_3N_4–SiC composites were bar shaped ($3 \times 3 \times 15\,mm^3$). The SiC content and the density of each composite is reported in Table 1.

3 Experimental Procedure

3.1 Heat treatments

The three materials SN-0, SNC-17 and SNC-34 (Table 1), were heat-treated under a controlled atmosphere. Samples were set into a graphite crucible on a platelet made from the same composite to avoid the diffusion of graphite into the sample. They were annealed in nitrogen atmosphere under $P = 0{\cdot}1$ MPa to prevent the decomposition of Si_3N_4.

To follow the evolution of the microstructure, four times of annealing (14, 30, 72 and 120 h) and three temperatures (1523, 1573 and 1623 K) were selected.

3.2 Indentification of the phases

Several techniques are necessary to identify the phases through annealing treatments: X-ray diffractometry (XRD), transmission electron microscopy (TEM at 100 keV), electron diffraction associated with TEM bright field–dark field images, X-ray energy dispersive spectrometry (EDS) in a TEM at 200 kV and irradiation damages induced by the electron beam during the TEM observations.

TEM observations were realized on thin foils prepared according to the classical procedure: samples 150-μm thick were cut with a diamond saw, mechanically thinned down to 80-μm and then ion milled.

3.3 Creep experiments

The samples were crept under uniaxial compression. They were cut off from either as-sintered or from annealed bars. Their size was $1{\cdot}5 \times 2{\cdot}5 \times 5$ mm. Creep experiments were performed at 1523 K under a load of 500 MPa and a flowing N_2 atmosphere (5 litres/h). Samples were weighed before and after the creep experiments to demonstrate that the decomposition of the composite was effectively negligible.

4 Results

4.1 Composition of the as-sintered materials

X-ray diagrams were obtained for the three variants, SN-0, SNC-17 and SNC-34. The major phases identified are β-SiC and β'-Si_3N_4, which consists of β-Si_3N_4 in which some Al and O are substituted for Si and N respectively. As an illustration, part of the diagram obtained with the SNC-17 composite is shown in Fig. 2(A). Some peaks of low intensity are also detected. They can be assigned to a mullite phase ($3Al_2O_3 . 2SiO_2$).

The repartition and size of the crystalline components was previously described.[3] It was shown that the materials also contain large intergranular glassy interphases (Fig. 1). The intergranular phases were analysed by electron energy loss spectroscopy (EELS) in the SNC-17 and in the SNC-34 composites. They contain Al, Y and O, as expected, due to the composition of the oxide additives, and also some amount of Si, N and C which are dissolved in the liquid oxide phase during the sintering.

4.2 Devitrification of the glassy phase in the composites

The annealing conditions were investigated to obtain the best devitrification of the glassy phase. The influence of time and of temperature was thus studied in the SNC-17 composite which contains an intermediate content of SiC.

4.2.1 Influence of the annealing time on the devitrification

X-Ray diagrams were obtained from the composite SNC-17 annealed at 1523 K during $t = 14, 30, 72$ and 120 h respectively. They show the following:

(i) The annealings result in the formation of two new crystalline phases (Fig. 2(B)): the yttrium disilicate ($Y_2O_3 . 2SiO_2$) called Y2S, and the yttrium and aluminium garnet ($3Y_2O_3 . 5Al_2O_3$), called YAG.

(ii) No change in the X-ray diagram is observed when the annealing exceeds 72 h: a diagram comparable to the one shown in Fig. 2(B) is obtained after a 120-h annealing.

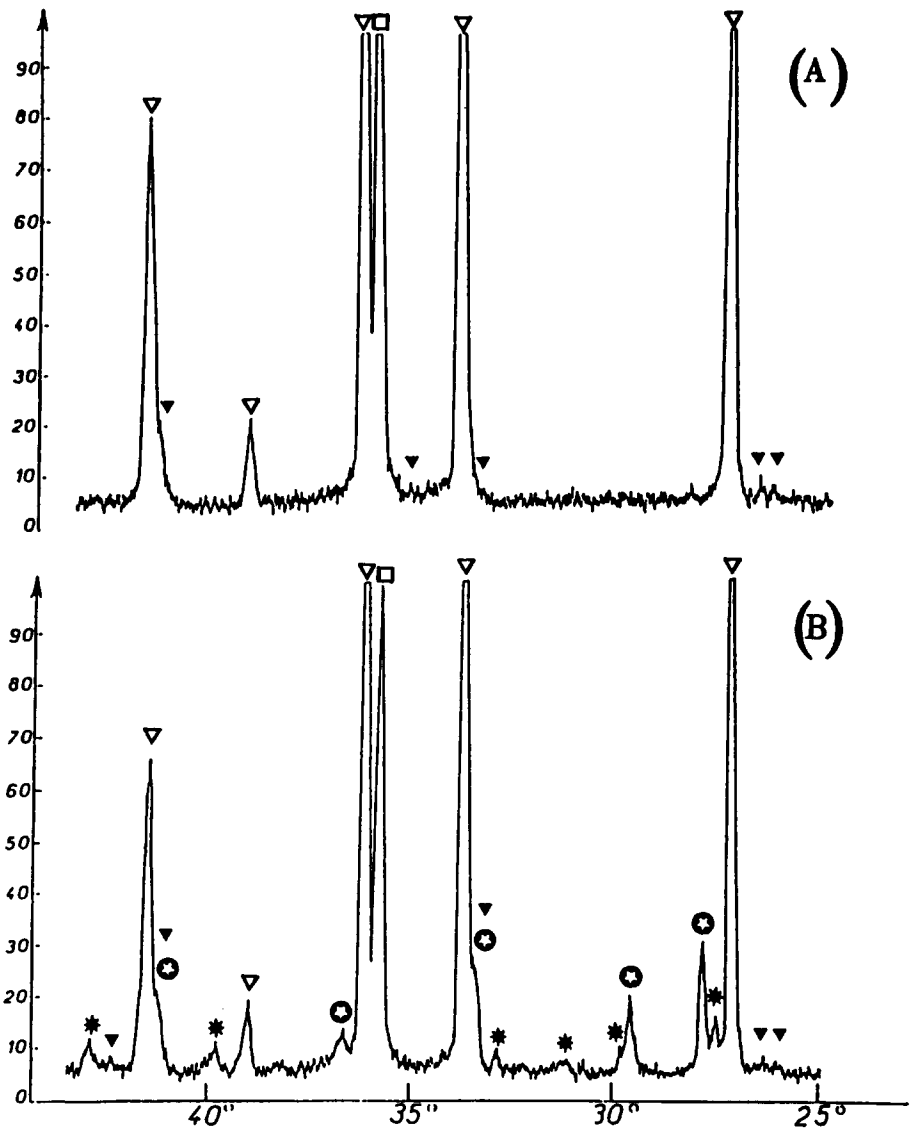

Fig. 2. X-Ray diffraction diagrams of SNC-17 composite (A) as-sintered and (B) annealed 72 h at 1523 K. In (A) β'-Si_3N_4 (▽), β-SiC (□) and mullite (▽) are the only crystalline phases detected. In (B), additional reflections characteristic of YAG ($3Y_2O_3 . 5Al_2O_3$, ✪) and of Y2S ($Y_2O_3 . 2SiO_2$, ★) are observed.

4.2.2 Influence of the annealing temperature on the devitrification

According to the X-ray diffraction, no further devitrification occurs after 72 h at 1523 K. Such an annealing time has therefore been selected to study the influence of the temperature on the devitrification.

—Annealing at $T = 1523$ K: As already mentioned, the heat-treatment results in the crystallization of YAG and Y2S. As shown in Fig. 2(B), more YAG than Y2S is formed during the devitrification.

—Annealing at 1573 K and at 1623 K: YAG alone is detected after heat-treatments at temperature equal to or higher than 1573 K (Fig. 3). Moreover, less YAG is formed at 1573 K than at 1523 K as shown by the peak intensities.

4.2.3 Stability of the phases formed by devitrification

The nature and the amount of the phases formed by devitrification depend on the annealing temperature. Annealed samples were thus submitted to a second 72-h annealing at higher or lower temperature than the first heat-treatment to check a possible evolution of these phases.

—Annealing at 1573 K after an annealing at 1523 K: A higher temperature of annealing does not induce any change in the X-ray diagram. X-Ray diffraction suggests that annealing at 1523 K results in a maximum devitrifica tion and shows that the phases obtained are stable.

—Annealing at 1523 K after an annealing at 1573 K: After this decrease in temperature and a subsequent annealing at 1523 K, the intensity

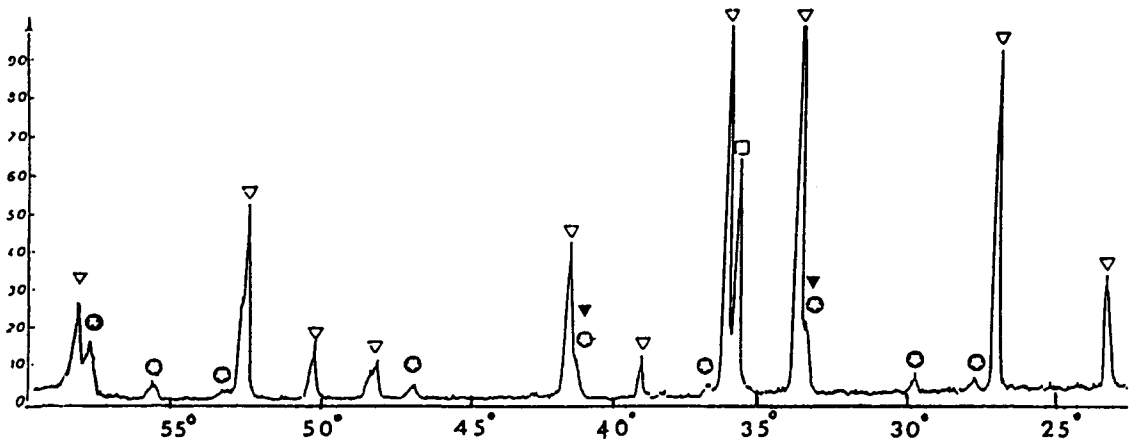

Fig. 3. XRD diagram of SNC-17 composite annealed 72 h at 1573 K. β'-Si_3N_4 (▽); β-SiC (□); YAG (✪).

of the YAG peaks increases and the Y2S peaks appear. Therefore, an annealing at 1573 K induces a less complete devitrification than at 1523 K. In addition, it does not favour the formation of Y2S.

4.2.4 Localization of the phases formed by devitrification

TEM observations show that the intergranular phase surrounding the β'-Si_3N_4 and β-SiC grains has almost completely crystallized during a 72-h annealing at 1523 K.

The YAG phase ($3Y_2O_3 . 5Al_2O_3$) was identified in pockets which contain SiC inclusions or which communicate with such pockets. The YAG forms large grains ($\sim 1\ \mu m$) as shown by electron diffraction (Fig. 4(a) and (b)). One single crystal develops at the expense of a glassy interphase of complex shape, which extends over one or two microns. The EDS spectra (Fig. 4(d)) exhibit the Al $K\alpha$ and Y $L\alpha$ peaks as well as a Si $K\alpha$ peak, whose intensity varies from grain to grain. The analysis is influenced by the surrounding SiC and $\beta'Si_3N_4$ grains. The Si detected may be due to this influence but it may also be related to a possible substitution of Al by Si.

The Y2S phase ($Y_2O_3 . 2SiO_2$) was identified in

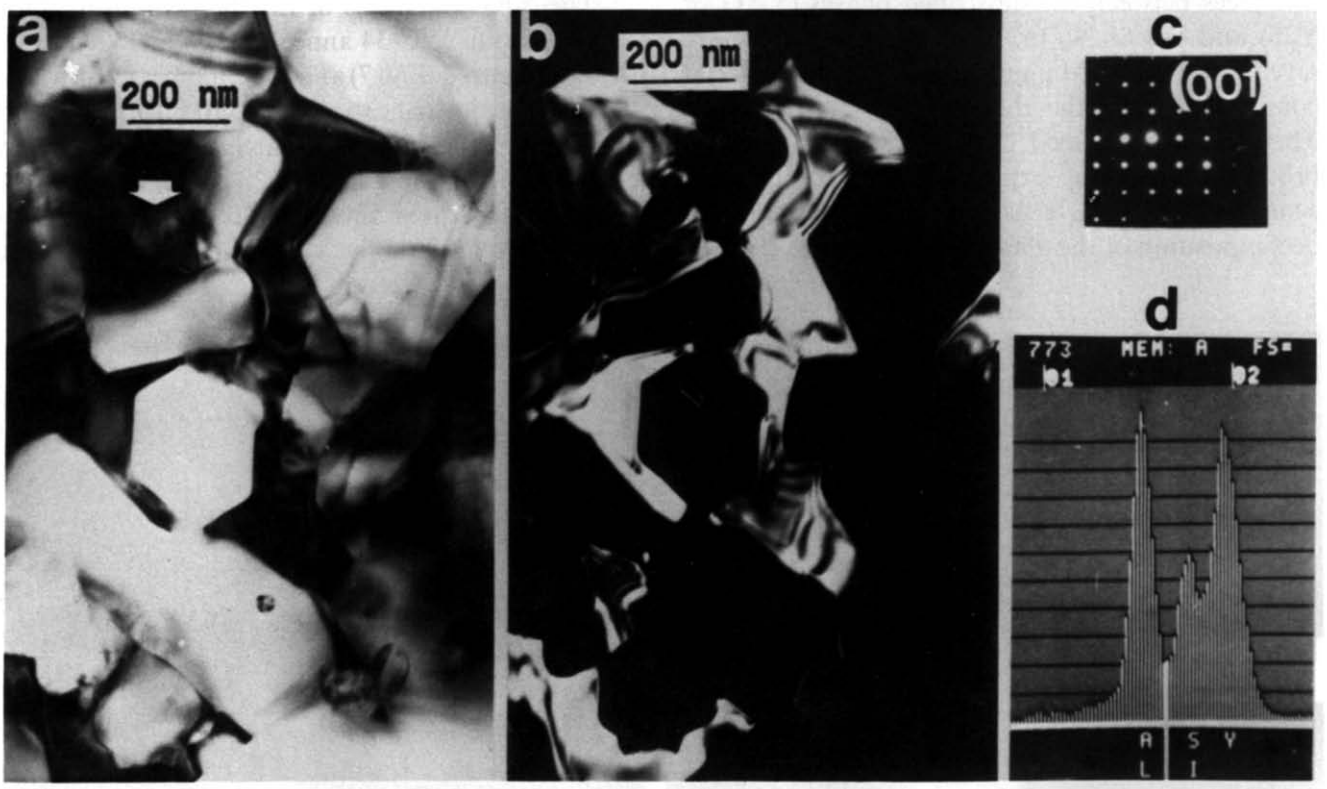

Fig. 4. Identification and localization of the YAG phase by TEM and EDS. (a) Bright-field, (b) dark-field images and (c) electronic diffraction pattern of a YAG grain formed by devitrification at 1523 K of the glassy interphase; (d) EDS spectrum of a YAG grain. In (a) the arrow localizes the SiC inclusion.

Fig. 5. Identification and localization of the Y2S by TEM and EDS. (a) Bright-field showing different Y2S grains (different arrows) formed by devitrification at 1523 K of the glassy interphase; (b) EDS spectum.

pockets exempt from SiC inclusions. It forms grains much smaller than the YAG ones (~ 200 nm, cf. Fig. 5(a)). The same glassy pocket devitrifies in several crystals. When the Y2S grains are rather large and next to the foil edge, the Si $K\alpha$ and Y $L\alpha$ peaks observed on the EDS spectra exhibit the same intensity (Fig. 5(b)). A very small Al $K\alpha$ peak is also observed.

Residual vitreous phases are observed after annealing at some triple junctions or at some interfaces between the devitrified phases (YAG or Y2S) and the Si_3N_4 or the SiC grains. They are revealed on the TEM images due to the difference of contrast between the different phases (Fig. 6(a)). They are also revealed by the irradiation damage produced by a long exposure under the electron beam (Fig. 6(b)). It is well known that the decomposition of the glassy oxides releases gaseous oxygen and results in the formation of bubbles in the glass.[13]

4.3 Influence of SiC on the devitrification of the intergranular phase

As previously mentioned, the intergranular phase may contain some carbon whose amount is likely to be related to the SiC content of the materials. It was thus necessary to check the possible influence of SiC on the devitrification.

The XRD diagrams of the three variants, SN-0, SNC-17 and SNC-34 annealed 72 h at 1523 K were thus compared (Fig. 7) and the following was found. Firstly, the devitrification results in the formation of both YAG and Y2S in the three variants. Secondly, the intensity of most of the Y2S peaks is roughly the same in the three variants. The texture observed likely accounts for the variations. Thirdly, despite

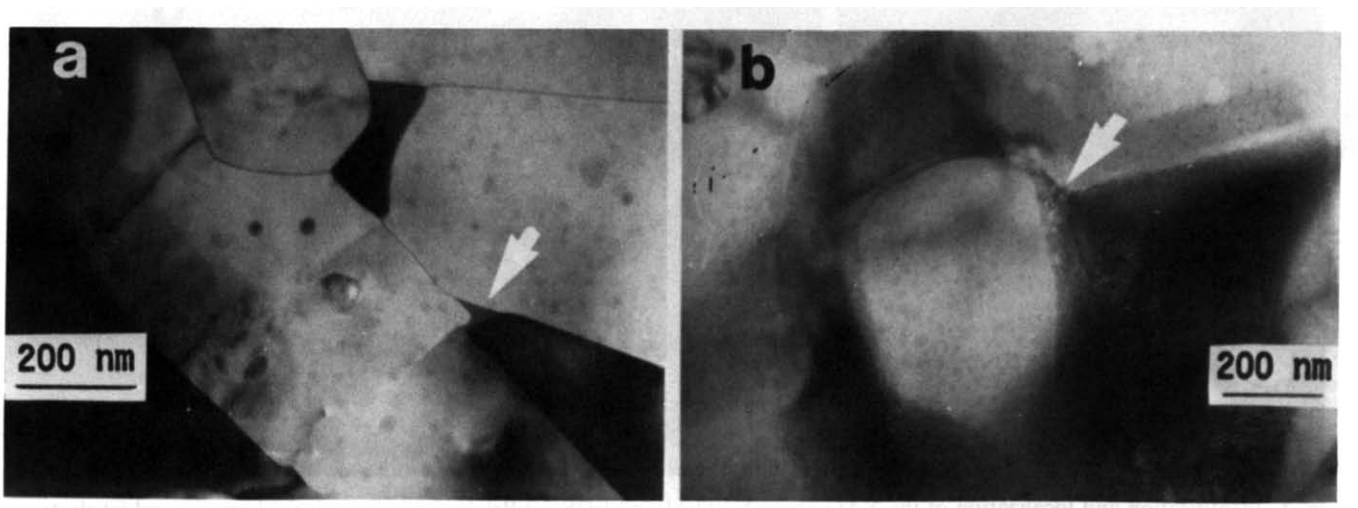

Fig. 6. Identification of the amorphous phase by TEM. Identification by (a) difference of contrast or (b) irradiation damages during TEM observations.

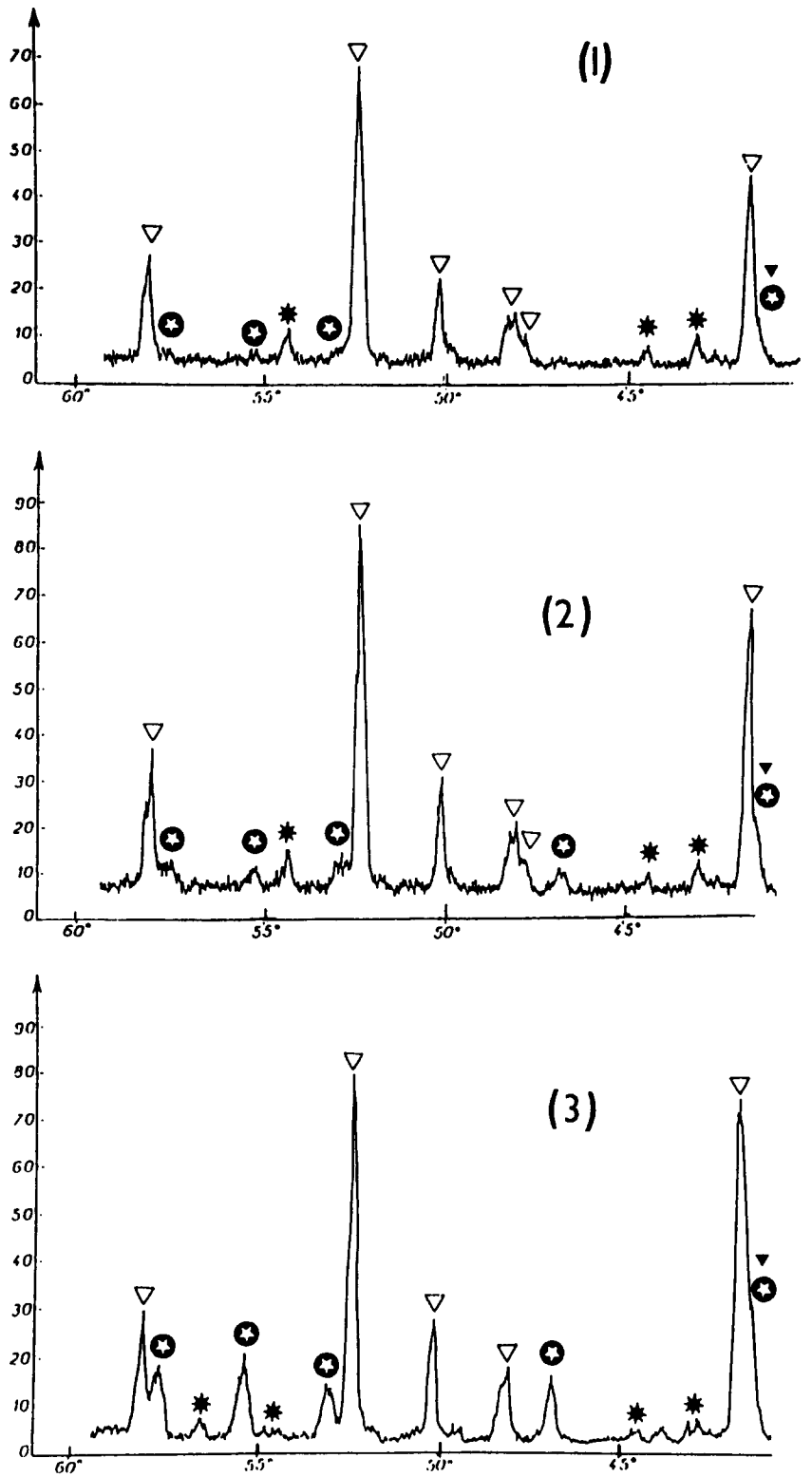

Fig. 7. XRD diagrams of materials annealed 72 h at 1523 K. (1) β'-Si_3N_4 (SN-0); (2) Si_3N_4–17 wt% SiC (SNC-17); (3) Si_3N_4–34 wt% SiC (SNC-34); β'-Si_3N_4 (▽); β-SiC (□); mullite (▽); YAG (✪); Y2S (★).

the texture, it is clear that the intensity of the YAG peaks increases when the SiC content increases.

As a result, it is possible to conclude that the addition of SiC influences the devitrification. It promotes a more complete devitrification and it is favourable to YAG formation.

4.4 Influence of the devitrification on the creep resistance

The devitrification depends on both the time and the temperature of the annealing. The variation of the creep resistance versus these parameters was thus investigated in the SNC-17 composite.

In the following, 'pre-annealing' denotes the annealing performed to promote the devitrification before the creep tests.

4.4.1 Influence of the pre-annealing time on the creep resistance

According to the X-ray diagram, a complete devitrification is achieved and the phases formed are stable after a 72-h pre-annealing at 1523 K. The influence on the creep resistance of the pre-annealing time was thus studied at this temperature. Creep was also performed at 1523 K.

The creep behaviour of SNC-17 composites pre-annealed during $t = 0$, 14 and 72 h was compared (Fig. 8). The un-annealed and the pre-annealed materials exhibit quite different behaviour.

The un-annealed composite firstly undergoes a rapid deformation. During this transitory stage, the deformation rate decreases rapidly (Fig. 9). After a few minutes and a deformation of roughly 0·5%, a short pseudo-steady-state stage is observed. During such a stage, the creep rate decreases very slowly, as observed in curve (a) of Fig. 9. Its value is approximately equal to $6 \times 10^{-7}\,s^{-1}$. When the deformation reaches about 1·2%, a tertiary creep stage is observed. The creep rate starts to increase rapidly and the sample breaks for a deformation of roughly 1·4%.

In the pre-annealed composites, after the transitory stage, a well-defined pseudo-steady-state stage is observed. This stage starts after a deformation of about 0·1 or 0·2% depending on the pre-annealing time (Fig. 8). During the pseudo-steady-state stage,

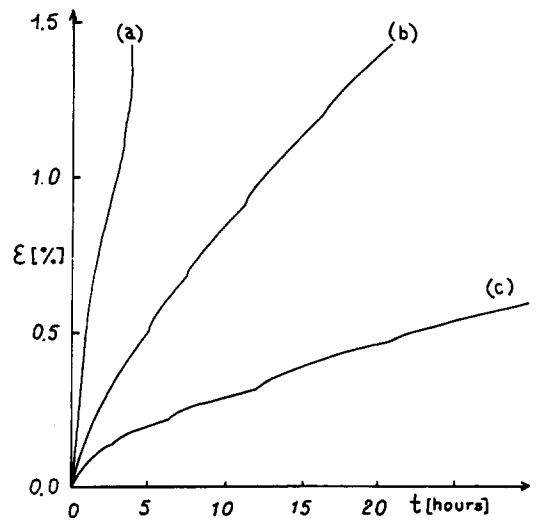

Fig. 8. Compression creep of SNC-17 composite at 1523 K. Relative deformation (ε) versus the time (t) under a 500 MPa applied stress. (a) Un-annealed composite; (b) and (c) composites pre-annealed 14 and 72 h respectively. Steep changes in the creep rate are observed during the deformation of the pre-annealed composites.

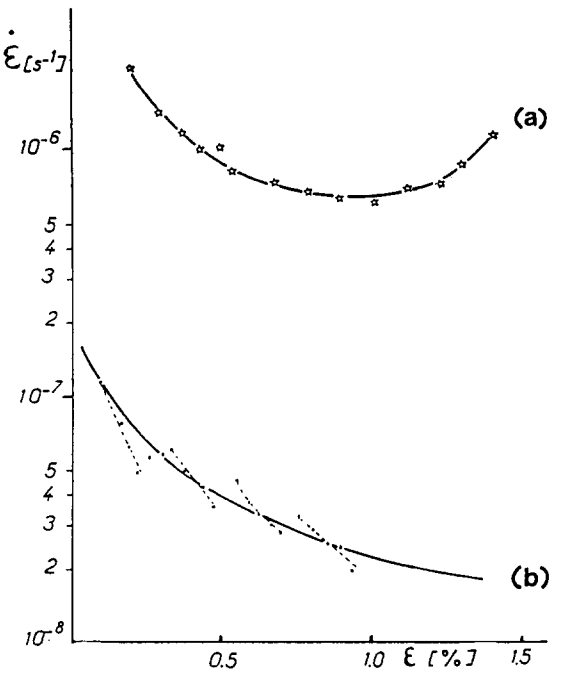

Fig. 9. The deformation rate ($\dot{\varepsilon}$) versus the deformation (ε) during the compression creep at 1523 K of SNC-17 composites. (a) Un-annealed composite; (b) composite pre-annealed 72 h at 1523 K.

the creep rate does not decrease regularly. From time to time, the deformation suddenly accelerates and then slows down again. These jumps of the deformation rates are observed whatever the pre-annealing time. A mean steady-state creep rate can be calculated. It is clearly lowered by pre-annealing. The longer the pre-annealing then the smaller the rate of deformation. It varies between 5 to $2 \times 10^{-8}\,s^{-1}$ in the sample pre-annealed for 72 h.

Whatever the pre-annealing time, no tertiary creep is observed for a 1·4–1·5% deformation.

4.4.2 Influence of the pre-annealing temperature on the creep resistance

The amount of devitrification and the resulting crystallized phases are different depending on the pre-annealing temperature (see Section 4.2.2). The influence of these different devitrifications on the creep resistance was thus investigated. The creep behaviour at 1523 K of SNC-17 pre-annealed 72 h at 1523 K or at 1573 K are compared in Fig. 10.

From a qualitative point of view, both curves exhibit the same features: a transitory stage is followed by a pseudo-steady-state stage. However, the slope changes on the deformation curves, that is to say the sudden increases of the deformation rate are more pronounced at 1573 K than at 1523 K. In addition the mean deformation rate during the pseudo-steady-state stage is higher at 1573 K than at 1523 K.

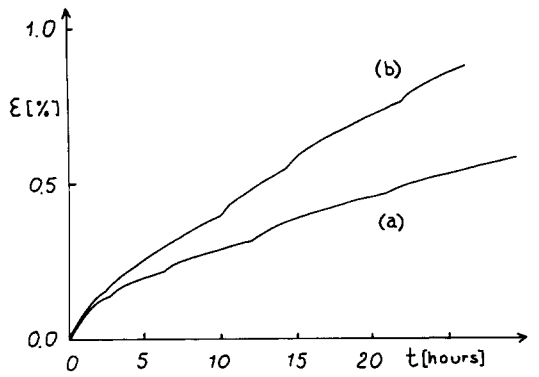

Fig. 10. Compression creep at 1523 K of SNC-17 composites under 500 MPa. The composites were pre-annealed 72 h at (a) 1523 K or (b) 1573 K.

5 Discussion

The applied heat-treatments modified the microstructure and the composition of the β'-Si_3N_4 and of the β'-Si_3N_4–SiC composites. The observed devitrification depends on mechanisms which will now be discussed. Its influence on the creep resistance will then be analysed.

5.1 Devitrification at 1523 K

5.1.1 Formation of YAG and Y2S

It was found that the microstructure of the devitrified intergranular phases differs depending on their composition. This variation implies that different mechanisms of crystallization are involved.

The Y2S phase appears to nucleate at a β'-Si_3N_4–glass interface. Several Y2S grains develop in the same intergranular pocket. The nucleation rate is thus likely to be greater than the growth rate. Considering the analogy between the Si–O and the Al–O bonds, some Al atoms may have been incorporated into the Y2S grains. The EDS spectra shown in Fig. 5 are compatible with such an assumption.

The YAG phase, in contrast, appears to nucleate at a SiC inclusion—glass interface. The nucleus grows, invading a large intergranular area. It seems quite obvious that the nucleation rate of the YAG is relatively low compared to its growth rate. It was previously shown that Si and N may be incorporated into the YAG phase.[14] The EDS spectra shown are compatible with such a result. Therefore, it appears to be likely that the variable substitution of the YAG level promotes the accommodation of some Si and N contained in the vitreous phase.

If the YAG phase nucleates at the SiC inclusion–glass interfaces, an increase of the density of these inclusions will result in an increase of the amount of devitrified YAG. The SiC inclusions are formed during the sintering by dissolution–precipitation of the SiC powder in the liquid oxide phase.[7] Their density is expected to increase, and thus the amount of YAG formed, with the SiC content in the composites. Such a correlation between the amount of YAG and the SiC content of the composites was indeed experimentally observed.

5.1.2 Residual vitrous phase

Microstructural observations have demonstrated that vitreous pockets and interfacial glassy films still persist in the SNC-17 annealed composite. Two mechanisms may originate in such residual vitreous phases.

During the devitrification, impurities (Ca, Fe, etc.) and atoms (C, Si, N) which cannot be incorporated into the growing Y2S or YAG grains are rejected into the liquid phase. If, locally, the concentration of these rejected elements grows too large, the residual liquid phase cannot crystallize. It remains in the materials either as pockets at the double or triple junction or as vitrous interphases. The size of the glassy pockets or interphases prevented their chemical analysis. However, this classical mechanism was probably operating during the devitrification.

When the devitrification results in a large volume increase it induces elastic stresses. These stresses slow down the crystallization. When they grow large enough they inhibit further devitrification.[15] The analysis of the creep experiments (cf. Section 5.3) suggests that such a mechanism accounts for the incomplete devitrification which results from a pressureless annealing.

5.2 Devitrification at 1573 K and 1623 K

A SiO_2–Y_2O_3–Al_2O_3 liquid eutectic exists at relatively low temperature. The lowest value reported is 1620 K.[16] The devitrification observed at 1523 K proves that such a melting temperature is not valid for the glassy phase studied. However, a softening of the glassy phase may occur at 1573 K and results in the slowing down of the devitrification as observed.

According to the X-ray diagrams, the growth rate of the Y2S is drastically decreased, or even inhibited, at $T \geq 1573$ K. Further studies are necessary to verify this observation.

5.3 Influence of the devitrification on the creep resistance

The detailed study of the creep behaviour of the SCN-17 un-annealed and pre-annealed composites demonstrates the efficiency of the devitrification in increasing the creep resistance.

The creep of the un-annealed composite is characteristic of a material containing a soft intergranular glassy phase. As previously mentioned, the glassy phase is close to its softening temperature at 1523 K. The low viscosity of the glassy phase reduces the friction between the grains making sliding easier. It has been shown that cavities develop under strain in phases of low viscosity,[17] resulting in the brutal rupture of the samples. Such a mechanism is likely to originate in the creep behaviour experimentally observed.

During creep at 1523 K of an un-annealed sample, devitrification must occur, probably accelerated by the stress. However, it is obviously too limited to modify the creep mechanism and to avoid rupture of the sample.

The creep behaviour of the pre-annealed composite is quite different. The pre-annealing has several consequences. It reduces the deformation during the transitory stage (0·1–0·2% versus 0·5% in the un-annealed sample). It results in well-defined pseudo-steady-state creep. It decreases the creep rate during this stage (a 72-h annealing at 1523 K divides $\dot{\varepsilon}$ by about 20). It avoids the occurrence of a tertiary creep for $\varepsilon \leq 1{\cdot}4\%$.

The beneficial effect of pre-annealing on the creep resistance increases with the amount of devitrification. Such an effect is demonstrated by the variation of the creep resistance with the pre-annealing time at 1523 K.

The crystallization of the interphases increases the resistance to the sliding between the grains, resulting in the hardening of the materials observed. However, the creep behaviour is not characteristic of a material exempt of glassy interfaces. The slope changes on the $\varepsilon = f(t)$ curves correspond to rapid grain rearrangements and subsequent hardening. Such microstructural changes are probably related to the residual glassy phase which was observed in pre-annealed samples. Under stress, the residual glassy phase flows towards regions submitted to lower stresses.[18] This viscous flow originates in rapid grain rearrangements. Moreover, the glassy phase submitted to lower stresses has the possibility to devitrify. These mechanisms result in a transitory stage and then in an hardening of the material. Such a model agrees with experimental results.

6 Conclusion

Heat-treatments conditions were investigated to devitrify the glassy intergranular phase and to stabilize the microstructure of β'-Si_3N_4 and β'-Si_3N_4–SiC pressureless sintered materials.

(1) Heat-treatments at 1523 K promote the best devitrification:
   (i) The microstructure is stabilized by a 72-h annealing. The devitrification results in YAG ($3Y_2O_3 . 5Al_2O_3$) and Y2S ($Y_2O_3 . 2SiO_2$) crystallization. Some intergranular glassy phases are left after the annealing. No further devitrification occurs when the annealing time is increased.
   (ii) SiC promotes a more complete devitrification and favours YAG formation.
   (iii) YAG forms large grains ($\sim 1\ \mu m$) next to SiC inclusions. It is likely to nucleate at a SiC–glass interface.
   (iv) Y2S forms small grains (~ 200 nm) in areas exempt from SiC inclusions. It is likely to nucleate at a β'-Si_3N_4–glass interface.

(2) Heat-treatments at 1573 K or 1623 K results in a less complete devitrification than at 1523 K. The YAG phase alone is detected.

(3) The devitrification increases the creep resistance of the material:
   (i) The primary creep is reduced.
   (ii) A well-defined pseudo-steady-state creep is obtained.
   (iii) The creep rate is much smaller in pre-annealed than in un-annealed materials (by a factor of 20).
   (iv) The stress induces further devitrification of the residual glassy phase.

(4) In devitrified materials, the residual glassy phase still appears to have a prevalent influence on the creep behavior.

References

1. Birch, J. M. & Wilshire, B., *J. Mat. Sci.*, **13** (1978) 2627–36.
2. Buljan, S. G., Baldoni, J. G. & Huckabee, M. L., *Am. Ceram. Soc. Bull.*, **66** (1987) 347–52.
3. Bradley, S. A. & Karasek, K. R., *J. Mat. Sci. Lett.*, **6** (1987) 791–4.
4. Jack, K. H., *J. Mat. Sci.*, **11** (1976) 529.
5. Lou, L. K. V., Mitchell, T. E. & Heuer, A. H., *J. Am. Ceram. Soc.*, **61** (1978) 392.
6. Iskoe, L. J., Lange, F. P. & Diaz, E. S., *J. Mat. Sci.*, **11** (1976) 908.
7. Lancin, M., Ramoul-Badache, K. & Sevelly, J., *Phil. Mag. A*, **58** (1988) 667–76.
8. Kossowsky, R., Miller, D. G. & Diaz, E. S., *J. Mat. Sci.*, **10** (1975) 983.
9. Karunaratine, B. S. B. & Lewis, M. H., *J. Mat. Sci.*, **15** (1980) 449.

10. Greil, O. & Weiss, J., *J. Mat. Sci.*, **17** (1982) 1571–8.
11. Ahn, C. C. & Thomas, G., *J. Am. Ceram. Soc.*, **66** (1983) 14–17.
12. Tanaka, H., Greil, P. & Petzow, G., *Int. J. High Technol. Ceram.*, **1** (1985) 107–18.
13. Laval, J. Y. & Wesmacott, K. H., *Elec. Microsc. Analysis, Int. Conf. Ceram.*, **52** (1979) 295.
14. Thorel, A. *et al.*, Atomic structure of interfaces in Sialon ceramics. In *Ceramics Microstructures 86*, ed. J. A. Pask & A. G. Evans. University of California, Berkeley, Plenum Publishing Corporation, New York, 1987, p. 253.
15. Raj, R. & Lange, F. F., *Acta Met.*, **29** (1981) 1993–2000.
16. Venables, J. D., McNamara, O. K. & Lye, R. G., *Nitrogen Ceramics*, ed. F. L. Filey. Noordhoff Press, Groningen, The Netherlands, 1977, p. 391.
17. Karunaratine, B. S. B. & Lewis, M. H., *J. Mat. Sci.*, **15** (1980) 449.
18. James, K. & Ashbee, K. H. G., *Prog. Mat. Sci.*, **21** (1975) 1.